# Off-Design Performance of an Organic Rankine-Vapor Compression Cooling Cycle using R1234ze(E)

**Alex Grauberger[a], Derek Young[a], Todd Bandhauer[a,*]**

[a] REACH CoLab, Colorado State University, Fort Collins, CO 80524, USA

* Corresponding author. Colorado State University, Department of Mechanical Engineering, 1374 Campus Delivery, Fort Collins, CO 80523, USA. E-mail address: tband@colostate.edu

## Abstract

In this study, a 264 $kW_{th}$ organic Rankine-vapor compression cycle (ORVC) was experimentally tested over a range of conditions to quantify the individual impact of off-design external conditions. The ORVC was designed to recover waste heat at 91°C, reject heat to a liquid condenser stream at 30°C, and produce chilled water at 7°C. The condenser heat rejection temperature was varied from 16.6°C to 32.6°C, the chilled water delivery temperature was varied between 2.1°C and 13.1°C, and the heat input temperature was varied from 91°C to 120°C. As the condenser heat rejection temperature decreased, the coefficient of performance (COP) of the ORVC improved from 0.558 at 30°C to 0.682 at 16.6°C, despite a reduction in compressor isentropic efficiency. Although the chilled water temperature variation had almost no impact on the organic Rankine cycle performance, the compressor efficiency decreased when the delivery temperature was below 7°C. At the highest chilled water temperature, 13.1°C, the COP of the ORVC was 0.643. Compressor stall was noted when the condenser heat rejection temperature was greater than 32.6°C and the chilled water delivery temperature was below 2.1°C. Increasing the driving heat source inlet temperature improved the COP of the ORVC and the thermal efficiency of the organic Rankine power cycle, while decreasing the efficiency of the compressor and the COP of vapor compression cycle. In addition, the integrated part load value of the system was determined through experimentation to be 0.682, which provides a realistic estimate of real-world performance.

**Keywords: Waste heat recovery, Thermally activated cooling, Off-design performance, Experimental demonstration**

| ***Nomenclature*** | | ***Subscripts*** | |
|---|---|---|---|
| AHRI | Air Conditioning, Heating, Refrigeration Institute | boiler | Boiler |
| COP | Coefficient of performance | comp | Compressor |
| GHG | Greenhouse gas | cond | Condenser |
| GWP | Global warming potential | in | Inlet |
| HVAC | Heating, ventilation, and air conditioning | deliv | Delivery |
| IPLV | Integrated part load value | TH | Thermal |
| ORC | Organic Rankine cycle | ORC | Organic Rankine cycle |
| ORVC | Organic Rankine-vapor compression | out | Outlet |
| PID | Proportional-integral-derivative | turb | Turbine |
| SC | Subcooled | VC | Vapor compression cycle |
| SH | Superheated | 2nd | $2^{nd}$ Law efficiency |
| SLHX | Suction line heat exchanger | | |
| TP | Two-phase | | |
| VCC | Vapor compression cycle | | |
| VFD | Variable frequency drive | | |

***Variables***

| | |
|---|---|
| $COP$ | Coefficient of performance [-] |
| $h$ | Enthalpy [kJ kg$^{-1}$] |
| $\dot{m}$ | Mass flow rate [kg s$^{-1}$] |
| $\dot{Q}$ | Heat duty [kW] |
| $T$ | Temperature [°C or K] |
| $\dot{V}$ | Volume flow rate [m$^3$ s$^{-1}$] |
| $\eta$ | Efficiency [-] |
| $\rho$ | Density [m$^3$ kg$^{-1}$] |

**Highlights**

Experimental off-design performance of an organic Rankine-vapor compression cycle.

Integrated part load value for thermally activated cooling system.

Characterize operational envelope for ORVC test facility.

## 1. Introduction

The generation of power (mechanical or electrical) with fossil fuels is typically 30-35% efficient while the remaining 65-70% of the fuel energy is released as waste heat. Capturing waste heat energy from fuel driven prime movers and converting it to useful energy (mechanical, electrical, or cooling) is one method to reduce greenhouse gas (GHG) emissions. Industrial waste heat from process heating and on-site boilers accounted for 3.12 x $10^9$ GJ in the U.S. manufacturing sector in 2014 which is another source of potential GHG reduction if it can be economically recovered [3]. One method to improve the energy efficiency of manufacturing plants is to capture the low-grade waste heat from prime movers, on-site boilers, or process heating and convert it to cooling using thermally activated cooling systems, thus reducing energy expenditures and GHG emissions. For example, 20% of the U.S. manufacturing sector electricity consumption is used for facility HVAC or process cooling/refrigeration (approx. 0.52 x $10^9$ GJ year $^{-1}$), which often have co-located boilers and prime movers for standby or prime power [2]. Although a significant amount of waste heat in the U.S. manufacturing sector exists at temperatures below 125°C (approximately 2.43 x $10^9$ GJ year$^{-1}$), very few thermally driven technologies can cost-effectively capture low temperature waste heat [4]. A promising type of thermally activated cooling system is the organic Rankine-vapor compression cycle (ORVC), where an organic Rankine cycle (ORC) directly drives a vapor compression cycle (VCC). In the ORVC, waste heat vaporizes an organic working fluid, which is then expanded in a turbine on the ORC to produce useful mechanical power. The power output from the turbine is used to power the compressor, which drives the VCC to provide the useful cooling effect.

A recent study performed by Grauberger et al. designed, built, and tested a 264 $kW_{th}$ ORVC where the baseline performance was validated in accordance with AHRI standard rating conditions [5]. The Grauberger et al. study achieved a COP of 0.56 with a driving waste heat temperature of 91°C, a condenser heat rejection temperature of 30°C, and a chilled water delivery temperature of 7°C. The high-speed turbine and compressor had an extremely high shaft efficiency (nearly 100%), which contributed to the high COP for the testing conditions. Although the baseline performance was characterized in this study, off-design or part load operation accounts for ~99% of the operating hours of chillers, engines, and other equipment [6,7]. Chilling equipment is generally sized to meet the maximum expected loads for a specific application but are rarely subjected to such conditions. In addition, environmental conditions are constantly fluctuating, which will impact the performance of a thermally driven chiller.

There are numerous analytical studies available in the open literature that examine the off-design performance of organic Rankine-vapor compression cycles. For example, Kim and Blanco showed that increasing turbine inlet pressure will improve the cooling capacity at the cost of increased heat exchanger sizes with R134a [8]. Li et al. performed a parametric analysis on an ORVC which showed that higher coefficient of performance (COP) could be achieved by increasing waste heat temperatures, increasing evaporator temperatures, or decreasing the condenser temperatures [9]. A parametric simulation study from Bu et al. showed that the ORC turbine decreased in size as the heat source inlet temperature increased due to a larger enthalpy drop across the device, and the VCC COP decreased as a function of increased condenser temperature [10]. Yue et al. analyzed the performance of an ORVC integrated with an automotive diesel engine to find that condenser saturation temperature had the largest impact on the ORVC performance [11]. Molés et al. performed a parametric study of an ORVC with three methods of heat recuperation and found that R1234ze(E) had the best performance on the VCC and contributed more energy in the cross-cycle heat exchanger which improved the performance of the ORC [12].

Although these works incorporate parametric studies to show the impact of changing conditions on performance, none of the studies validated their models with experimental work. It is impossible to verify that the models represent real-world behavior without experimental performance characterization. These studies make many simplifying assumptions for heat exchanger and turbomachinery off-design performance which may not be representative of real-world performance. Further, many of the models allow heat exchanger and turbomachinery physical size parameters to vary as a function of the parametric variables, which is not a realistic indicator of actual performance. There are many competing factors when analyzing off-design that are not accounted for in many of these simulations, including: heat exchanger performance with fixed size at varying pressures and flow rates, dynamic effects between compressor load and turbine speed, turbomachinery off-design performance, heat loss/leakage, pump cavitation, and pressure drop.

Although analytical studies have demonstrated the viability of ORVC systems for heat activated cooling, but there are very few experimental ORVC studies that characterize thermodynamic performance over a range of conditions that are relevant to real-world, commercial operation. Prigmore and Barber (1975) tested a 10.5 $kW_{th}$ ORVC with a radial turbine and piston compressor connected via a gearbox [13]. Results from the study showed a 40% decrease in thermal COP as the temperature of the heat source was decreased from 101.7°C to 79.4°C. The next study from Biancardi et al. (1982) collected field data for a solar-driven ORVC heat pump installed in a commercial building in Phoenix, AZ to provide 70 $kW_{th}$ of chilled water [14]. The field data showed that the system could adequately respond to the transient cooling and heating needs of the building during typical daily cycling with hot water driving temperatures between 120°C and 160°C and chilled water delivery temperatures from 5.0°C to 12.5°C.

The experimental ORVC study from Wang et al. (2010) demonstrated a 4.4 $kW_{th}$ cooling capacity using a scroll expander driven by waste heat at 190°C [15]. In this study, results showed that increasing the pump speed on the ORC increased both the mass flow rate and the pump outlet pressure, which contributed to higher expander power output. The authors specifically highlight that changing one input in a physical system often affects a multitude of others, which is unlike simulation efforts where it is simple to alter a single parameter.

Demierre et al. (2014) designed an ORVC heat pump to generate 40 $kW_{th}$ of heating using a waste heat stream up to 123°C [16]. The heat pump operated over a range of heat source temperatures, condenser temperatures, and evaporator temperatures to find operational limits. At a condenser temperature of 34°C and an evaporator temperature of 3°C, the compressor began to surge due to turbo-compressor instabilities at higher rotational speeds and pressure ratios, an important result that was not captured by initial modeling estimates. Unfortunately, multiple external stream temperatures were changed in each test run, making it difficult to quantify the individual impact.

The study by Garland et al. in 2018 evaluated an ORVC designed to generate 250 $kW_{th}$ of chilled water at 16°C from low-grade waste heat at 106°C [17]. The ORVC was tested over a range of conditions and a high-fidelity performance prediction model was created with off-design performance data using heat exchanger scaling and turbomachinery scaling methods. Although this was one of the only experimentally validated modeling efforts to predict off-design performance, the experimental work did not determine the impact of individual external stream conditions on performance.

A recent experimental study by Liang et al. in 2021 quantified the performance of an ORVC designed to provide 1.8 $kW_{th}$ of refrigeration at -4°C over a range of conditions [18]. Unsurprisingly, the compressor speed and VCC mass flow rate increased as the condenser cooling temperature decreased since the compressor lift was reduced. The system was able to stabilize to steady state within 2 minutes after a 60% change in power cycle pump speed, which was the first published examination into transient performance for a small-scale ORVC.

Each of the works listed above performed experimental testing of ORVCs over ranges of conditions that did not align with rating standards for real operation of commercially available chillers. In addition, these studies often varied multiple inputs which made it impossible to quantify the performance impact of individual parameters. The performance of ORVC systems should be quantified when subjected to changing external stimuli, such as driving heat source temperature, ambient temperature, or chilled water inlet temperatures.

This study will characterize the performance of the system presented by Grauberger et al. over a range of external conditions and calculate the integrated part load value (IPLV) of the ORVC [5]. The IPLV is an industry standard performance metric used to assess the turndown performance capabilities of chillers at conditions representative of real-world operation. The present work builds upon the efforts of Grauberger et al. by experimentally quantifying the off-design performance of the same 264 $kW_{th}$ ORVC test facility. As a result, the performance testing in this study provides insights on the expected real-world performance of the ORVC over a range of conditions.

## 2. Experimental Methods

### 2.1. Organic Rankine-Vapor Compression Cycle Working Principle

A process flow diagram of the system is given in Fig. 1. The ORVC incorporated three methods of heat recuperation and a directly coupled turbo-compressor to enhance thermodynamic performance. On the organic Rankine power cycle (ORC), the working fluid R1234ze(E) was vaporized by hot glycol in the waste heat boiler. Then, the superheated vapor was expanded in the radial turbine to produce mechanical power. The rotating turbine shaft was directly connected to the centrifugal compressor wheel on the VCC. After expansion in the turbine, some remaining sensible energy in the working fluid was recovered in a recuperative heat exchanger, which heated the fluid at the power cycle pump outlet. The recuperator decreased the amount of external heat required to bring the working fluid to the desired temperature in the boiler, which

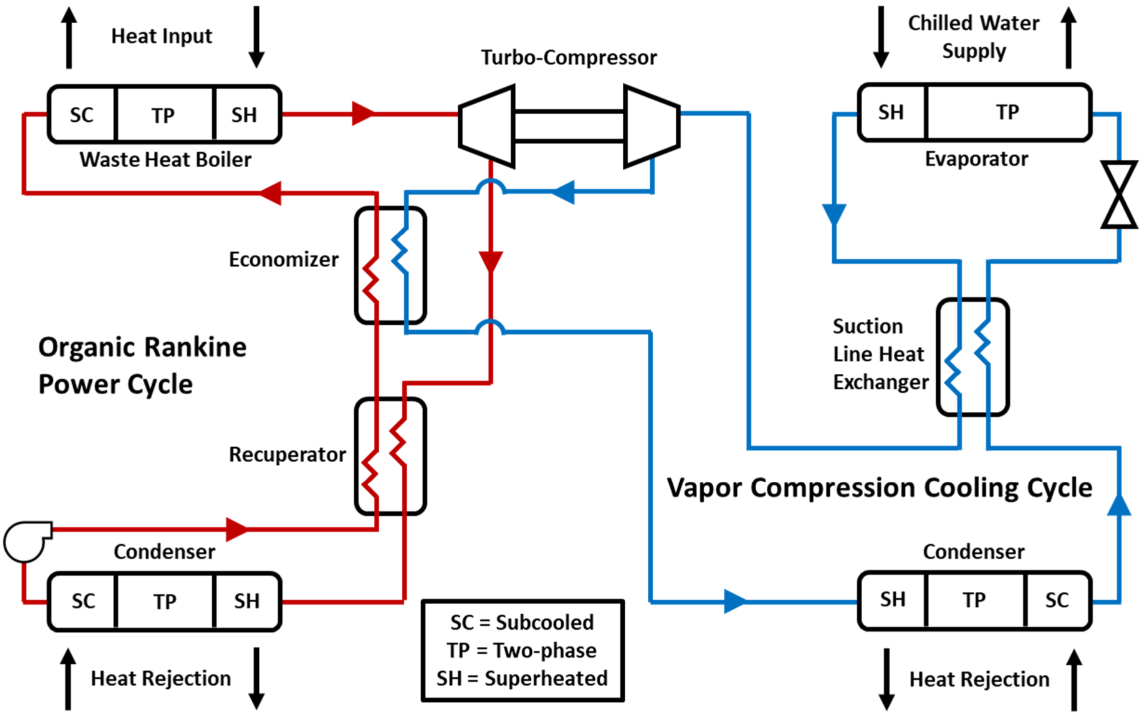


**Fig. 1.** Process flow diagram of the organic Rankine-vapor compression test facility. "SC" represents the heat exchanger area where the refrigerant is subcooled, "TP" represents the two-phase region of the heat exchanger on the refrigerant side, and finally "SH" represents the region where the refrigerant is a superheated vapor.

improved the efficiency of the ORC. After heat recuperation, the working fluid was fully liquefied in a condenser, which rejected heat to a liquid glycol stream. The liquid glycol condenser loop ultimately rejected heat to the ambient outdoor air in a hybrid evaporative cooling tower that provided glycol at 30°C, at the design point. The working fluid was pressurized in a refrigerant pump, preheated by the recuperator and economizing heat exchanger (economizer), and then vaporized in the boiler to complete the cycle.

On the VCC, R1234ze(E) was pressurized by the compressor. The power cycle fluid, prior to the boiler inlet, was preheated by the high temperature and pressure compressor discharge in the economizer. The compressor discharge had considerable sensible energy because a suction line heat exchanger (SLHX) was incorporated. The heat recovery in the economizer further decreased the heat input required by the ORC to generate the same amount of power in the turbine, which provided an additional improvement to the ORC thermal efficiency. Following the economizer, the working fluid was completely liquefied and subcooled in the condenser by rejecting heat to a liquid glycol stream. The subcooled working fluid entered the SLHX and transferred heat to the refrigerant prior to compressor inlet, which further subcooled the liquefied working fluid. Then, the liquid was throttled in the expansion valve to greatly decrease the temperature and pressure, where it also became a two-phase mixture. The two-phase R1234ze(E) absorbed heat from an external water stream to become a superheated vapor in the evaporating heat exchanger (evaporator), which produced the desired chilling effect. The vaporized working fluid was further superheated in the SLHX from the higher temperature liquid stream at the condenser outlet. In addition to increasing the latent cooling in the evaporator, the SLHX prevented liquid droplets from entering the compressor, which would damage the machine. Then, the refrigerant was pressurized in the compressor to complete the cooling cycle.

### 2.2. ORVC Test Facility Description

The ORVC test facility from Grauberger et al. was used for off-design testing in the present study. A brief overview will be provided here, while more detailed discussion, including a piping and instrumentation diagram, can be found in the original Grauberger et al. study [5]. The waste heat boilers, recuperators, suction line heat exchangers, and the cross-cycle economizer were aluminum brazed, plate fin style heat exchangers. Commercially available shell and tube heat exchangers were used for the power and cooling cycle condensers and the evaporator. The heat transfer area of the power cycle condenser and the cooling cycle condenser was 42.6 $m^2$ and 28.3 $m^2$, respectively. The heat transfer area of the evaporator was 19.0 $m^2$. Three boiler cores were used in parallel to ensure there was sufficient heat exchanger area to deliver 500 $kW_{th}$ of heat to the ORVC. Two recuperator cores and suction line heat exchanger cores were used in parallel to reduce refrigerant pressure drop. The fully operational test facility is shown in Fig. 2. The shell and tube heat exchangers had R1234ze(E) refrigerant on the shell side and the external stream (liquid glycol or pure water) in the tube side. The condensers used liquid ethylene glycol and the evaporator had pure water in the tubes. The centrifugal turbo-compressor was custom fabricated by Barber-Nichols, Inc. The turbocompressor was designed to operate at approximately 31,000

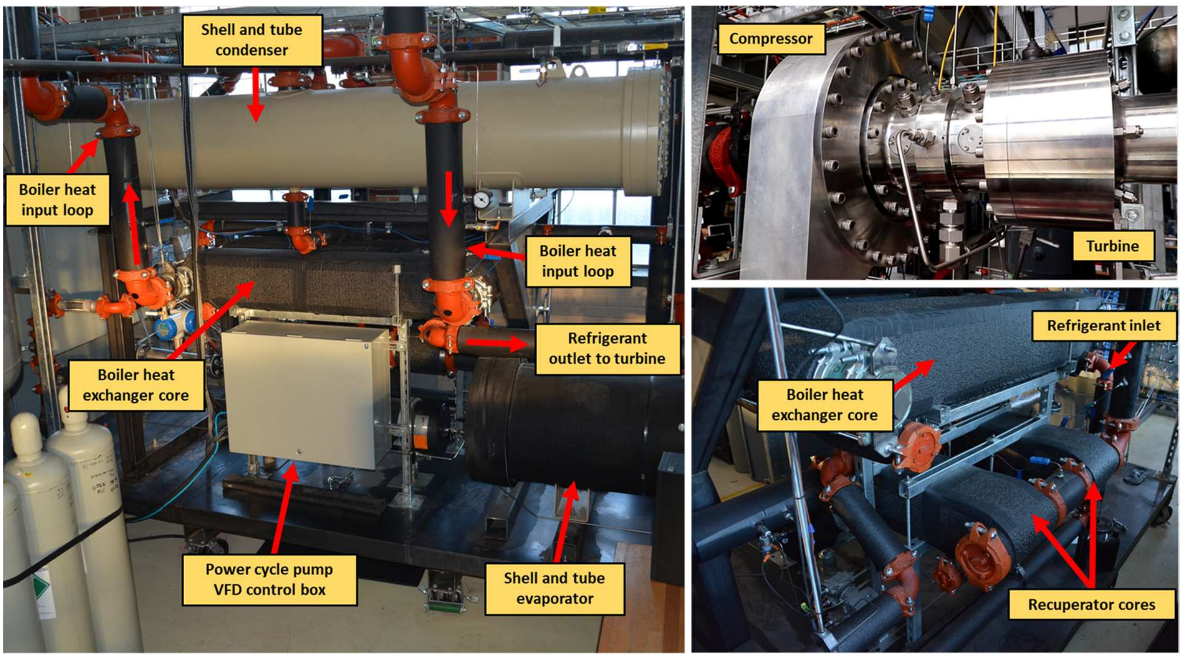


**Fig. 2.** ORVC test facility.

RPM, with a turbine power output of 52 kW at the design point. The working fluid on the power cycle was pressurized by a six-stage, side channel pump driven by a 19 kW three-pole motor with a VFD [19].

Three auxiliary loops were required to operate the test facility: waste heat simulation loop, chilled water simulation loop, and condenser heat rejection loop. An overview of each auxiliary loop is shown in Fig. 3. Pure water was pumped in the chilled water simulation loop (Fig. 3a) through the shell and tube evaporator, where it was chilled by the evaporating refrigerant. After chilling, the water was heated in a plate and frame heat exchanger with 60°C propylene glycol on the adjacent side. The temperature of the propylene glycol was maintained at 60°C in a natural gas-fired circulation heater and the flow rate was controlled with an electronic v-port ball valve. The flow of water in the evaporator was provided by a centrifugal pump and controlled with a gate valve. A 50% by volume mixture of ethylene glycol and water was pumped in the waste heat simulation loop (Fig. 3b) through the three parallel boiler cores to vaporize the R1234ze(E) working fluid. The glycol was heated in a secondary heat exchanger by a natural gas fired steam boiler (not shown) and six electric heaters. Glycol flow was generated by a high temperature centrifugal pump, while the flow rate was metered with a gate valve. 50% by volume ethylene glycol was pumped in the condenser loop (Fig. 3c) to the power and cooling cycle shell and tube condensers to absorb heat from the refrigerant. After the glycol absorbed heat in the condensers, it was cooled in a hybrid evaporative cooling tower (not shown), which sprayed water on coils

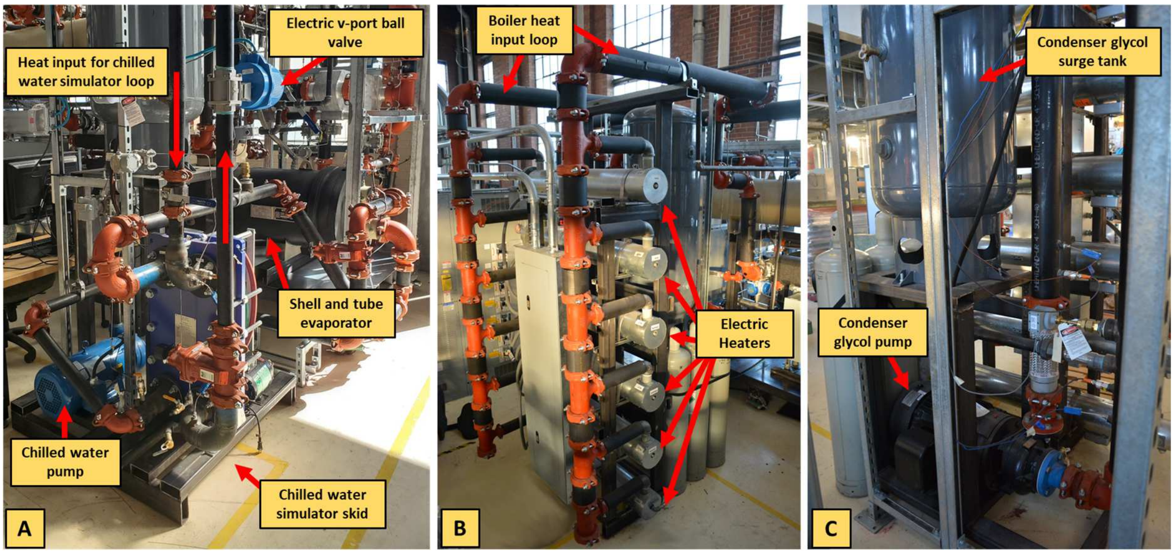


**Fig. 3.** Auxiliary loops for ORVC test facility.

containing the glycol. Air was pulled over the cooling coils to further reduce the temperature of the glycol by a fan mounted on top of the cooling tower. The temperature of the glycol at the cooling tower outlet was maintained at the set point using a PID on the variable frequency drive that controlled cooling tower fan speed.

The performance of the ORVC was quantified by measuring temperature, pressure, and flow rates on the ORC, VCC, and the three auxiliary loops. Temperature, pressure, or vapor mass quality were used in REFPROP to calculate enthalpy and entropy at each state point for the refrigerant in the ORVC [20]. Akasaka equations of state were used for R1234ze(E) [21]. The flow rate through the cooling cycle was calculated using an energy balance on the economizer, assuming heat loss to the ambient environment was negligible. The thermocouples and pressure transducers were calibrated over ranges relevant for the investigation following ASME PTC 19.1-2018 [22].

AHRI 551/591 and AHRI 560 performance rating standards for vapor compression chillers and absorption chillers were used to characterize the performance of the ORVC, based on data gathered from the external streams.

### 2.3. Baseline Performance

The baseline performance of the ORVC was quantified in a previous study which served as a comparison metric for the off-design performance testing [5]. The baseline data point was collected at 2 Hz over a 15-minute interval after steady state was reached, which conformed to the AHRI performance rating standards. The total uncertainty for the external loop state points values was less than 1% larger than the respective bias errors from extremely low systematic uncertainty. The AHRI precision and stability criteria were met for the flow rates and temperature measurements of the external streams. The condenser flow rate was 25.6% below the targeted design point value because the pressure drop through the piping network was too large for the pump to overcome. Fixing this would require a new pump and motor, which was too costly to justify at this stage of development.

The thermal COP of the ORVC was defined as the ratio of chilling heat duty to the amount of heat input, as shown in Equation (1).

$$COP_{\mathrm{TH}} = \frac{\dot{Q}_{\mathrm{evap}}}{\dot{Q}_{\mathrm{boiler}}} \tag{1}$$

The COP of the vapor compression cycle was determined by dividing the evaporator heat duty by the compressor power, shown in Equation (2).

$$COP_{\mathrm{VC}} = \frac{\dot{Q}_{\mathrm{evap}}}{\dot{W}_{\mathrm{comp}}} \tag{2}$$

The thermal efficiency of the ORC was the net work divided by the amount of heat input, shown in Equation (3).

$$\eta_{\mathrm{ORC}} = \frac{\dot{W}_{\mathrm{turb}} - \dot{W}_{\mathrm{pump}}}{\dot{Q}_{\mathrm{boiler}}} \tag{3}$$

The isentropic efficiency of the turbine, compressor, and power cycle pump were calculated with Equations (4) and (5), respectively.

$$\eta_{\mathrm{turb}} = \frac{h_{\mathrm{in}} - h_{\mathrm{out}}}{h_{\mathrm{in}} - h_{\mathrm{out,s}}} \tag{4}$$

$$\eta_{\text{comp}}, \eta_{\text{pump}} = \frac{h_{\text{out,s}} - h_{\text{in}}}{h_{\text{out}} - h_{\text{in}}} \tag{5}$$

Two different off-design testing procedures were carried out during this work: parametric study of external stream temperatures and integrated part load value (IPLV) testing. The data, unless otherwise noted, met the stability and accuracy criteria from the AHRI standards [6,23].

### 2.4. Parametric Testing of External Stream Temperatures

The off-design performance of the ORVC was characterized using AHRI 551/591 standard testing conditions for vapor compression-based water chillers and AHRI 560 standard rating conditions for absorption chillers. The performance of the system was characterized as a function of the auxiliary loop temperatures: condenser glycol inlet temperature, chilled water delivery temperature, and boiler glycol inlet temperature. Throughout parametric testing of different external stream temperatures, the amount of heat input was kept constant, while the amount of chilling provided by the ORVC varied as a function of auxiliary loop temperatures. The auxiliary loop temperatures were the most relevant conditions for quantifying off-design performance because they represent a change in the external environment in which the chiller is operating. For example, if the ORVC was recovering engine coolant waste heat from a diesel genset and the load on the diesel generator were to suddenly change, the amount of heat rejected to the condenser would change, resulting in cooling loop temperature fluctuations and off-design performance. It is critically important to understand how the ORVC responds to external stimuli

**Table 1**
Range of conditions for off-design testing.

| ***Parameter*** | ***Values*** | ***Increment*** |
|---|---|---|
| Condenser Glycol $T_{\text{in}}$ | 16.6°C to 32.6°C | 3.0°C |
| Chilled Water $T_{\text{deliv}}$ | 2.1°C to 13.1°C | 2.0°C |
| Boiler Glycol $T_{\text{in}}$ | 91°C to 120°C | 5.0°C |

and reliably predict technical performance.

Table 1 shows the ranges of auxiliary loop temperatures that were tested during this work while the flow rates were maintained at their baseline values. Although the AHRI 551/591 standard denotes the condenser inlet temperature should be tested from 12.8°C to 40.6°C, challenges with the test facility limited the temperature range during testing from 16.5°C to 32.6°C. As the condenser temperature decreased, the power output from the turbine increased and the cooling capacity was increased. Testing was limited on the low end of condenser temperatures because the external propylene glycol loop could not generate enough heat to maintain steady chilled water delivery temperatures. On the high end of condenser glycol temperature, the compressor stalled which made operation impossible. To alter the condenser glycol inlet temperature, the fan speed on the cooling tower was controlled with a VFD. Since a PID was used on the fan speed, the desired glycol temperature was set in the PID control logic and was allowed to stabilize until steady state was reached.

According to the AHRI 551/591 standard, the chilled water was required to be tested from 2.1°C to 21.1°C, but the auxiliary loops were only able to accommodate delivery temperatures up to 13.1°C. At the high end of evaporator water temperatures, above 13.1°C, the cooling capacity dramatically increased and again, the propylene glycol loop could not generate enough heat input to maintain steady state operation. To control the chilled water delivery temperature, the flow rate of 60°C propylene glycol from the natural gas heater was metered with an electronically controlled v-port ball valve.

Finally, the AHRI 560 standard for absorption chillers recommends the heat source temperature to be varied from 82°C to 204°C for testing, but the test facility components were not rated for safe operation above 120°C. Below 91°C, the test facility was physically limited by the size of the boiler. The three boiler cores could not fully vaporize the working fluid as a result of pinch point limitations. Although boiler inlet temperatures lower than 91°C could be tested by reducing the power cycle mass flow rate (and the saturation pressure in the boiler), the AHRI 560 standard requires the heat input to remain at 100% load during the parametric study of boiler temperatures. At the baseline case of 91°C, three of six electric circulation heaters were powered to provide heat to the glycol. Additional electric circulation heaters were cyclically powered to

**Table 2**
IPLV testing conditions.

| *Evaporator Duty* | *Condenser Glycol Inlet Temperature* |
|---|---|
| 100% | 30.0°C |
| 75% | 24.5°C |
| 50% | 19.0°C |
| 25% | 19.0°C |

match the required heat duty inputs for the test facility.

The temperatures of the external streams were changed in the increments as designated by the standards. Each off-design test was commenced after the ORVC stabilized to steady state and the data was collected over a 15-minute period at a sampling frequency of 2 Hz. For each test, a single auxiliary loop temperature was changed while the other two temperatures were held at their baseline values. In addition, the external loop flow rates were held at their baseline values throughout the testing procedures.

### 2.5. Integrated Part Load Value (IPLV) Testing

The integrated part load value (IPLV) of the ORVC system was determined in accordance with AHRI 551/591 standards. During IPLV testing, the $COP_{TH}$ of the ORVC was measured at different evaporator chilling loads and different condenser temperatures, as shown in Table 2. The IPLV is the industry standard method of measuring the overall average efficiency of a chiller and is defined in Equation (8):

$$IPLV = 0.01 \cdot A + 0.42 \cdot B + 0.45 \cdot C + 0.12 \cdot D \tag{8}$$

In Equation (8), *A* represents the $COP_{TH}$ at 100% load, *B* represents $COP_{TH}$ at 75% load, *C* represents $COP_{TH}$ at 50% load, and *D* represents $COP_{TH}$ at 25% load. AHRI determined the weighting factors in Equation (8) based on the average amount of time water-cooled VCC spend at each load. Although chillers are sized to meet the maximum possible load for an application, most of their operational life is spent at 50%-75% loads. As shown in Table 2, the AHRI standard for IPLV requires testing at reduced condenser temperatures as the chilling load is decreased. In some applications, lower ambient temperatures could reduce the amount of chilling required for a given end-use. Thus, the condenser temperature and evaporator chilling load are changed simultaneously. The 2$^{nd}$ Law efficiency of each test point during IPLV testing was calculated according to Equation (6).

$$\eta_{\mathrm{ORVC,2nd}} = \frac{COP_{\mathrm{TH}}}{COP_{\mathrm{Carnot}}} \tag{6}$$

The Carnot COP was defined according to Equation (7) where all temperatures are in Kelvin.

$$COP_{\mathrm{Carnot}} = \frac{1 - \dfrac{T_{\mathrm{in,cond}}}{T_{\mathrm{in,boiler}}}}{\dfrac{T_{\mathrm{in,cond}}}{T_{\mathrm{out,evap}}} - 1} \tag{7}$$

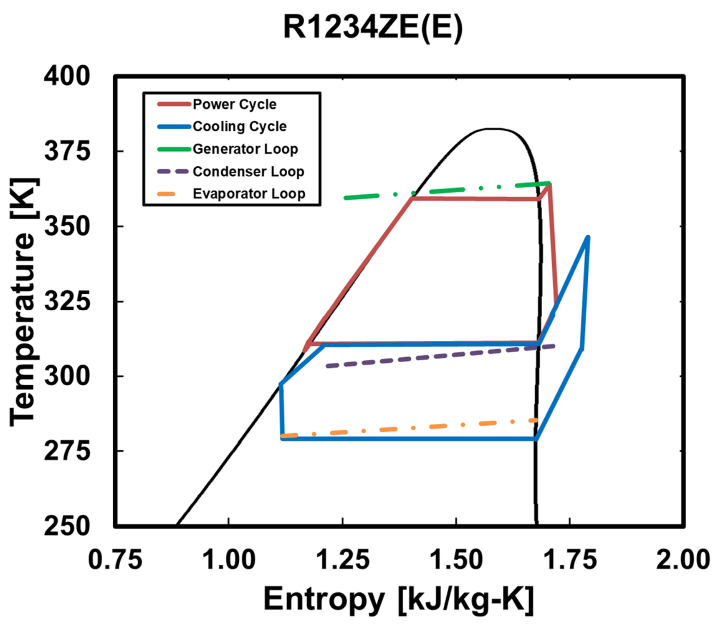


**Fig. 4.** T-s diagram for baseline ORVC performance.

## 3. Results and Discussion

### 3.1. Baseline Testing Results

The state points and steady-state performance metrics for the ORVC are shown in Fig. 4 and Table 3, which were calculated with the 15-minute averaged refrigerant state points and auxiliary loop state points from the Grauberger et al. study [5]. During the baseline testing, the thermal COP was 0.56 ± 0.01. The waste heat simulator loop input 473 kW ± 10.6 kW and the evaporator provided 263.8 kW ± 3.5 kW of chilling to the pure water stream. The turbo-compressor rotated at 31.5 kRPM with a power transfer efficiency of 100.3% ± 1.5%. The turbine generated 50.07 kW ± 0.57 kW with an isentropic efficiency of 76.7% ± 0.90%. The compressor used 50.24 kW ± 0.48 kW of power and had an isentropic efficiency of 84.75% ± 0.54%. The thermal efficiency of the ORC was 7.71% ± 0.22%, including pump work losses, and the COP of the VCC was 5.223 ± 0.09. The mass flow rate of the condenser glycol was the total flow rate of fluid through the two condensers. Additional results from baseline testing can

**Table 3.**
Baseline performance metrics for the ORVC.

| ***Parameter*** | ***Value*** |
|---|---|
| Boiler glycol $T_{in}$ | 91.00°C |
| Boiler glycol $\dot{m}$ | 26.87 kg $s^{-1}$ |
| Boiler glycol $\dot{Q}$ | 473.0 kW |
| Condenser glycol $T_{in}$ | 30.00°C |
| Condenser glycol $\dot{m}$ | 32.83 kg $s^{-1}$ |
| Evaporator water $T_{deliv}$ | 7.00°C |
| Evaporator water $\dot{m}$ | 12.57 kg $s^{-1}$ |
| Evaporator water $\dot{Q}$ | 263.8 kW |
| $COP_{TH}$ | 0.5577 |
| $COP_{VC}$ | 5.223 |
| $\eta_{ORC}$ | 7.706% |
| $\eta_{turb}$ | 76.70% |

be found in Grauberger et al [5].

### 3.2. Variable Condenser Inlet Temperature Results

The performance trends for the range of condenser inlet temperatures are shown in Fig. 5, along with a table that specifically highlights the overall performance metrics at the minimum and maximum test points for the condenser temperature. The baseline condenser temperature was 30°C. The baseline performance metrics are shown as 0% change on the plot in Fig. 5. The maximum COP achieved during condenser off-design testing was 0.682 which occurred at 16.6°C inlet temperature, from a combination of increased ORC thermal efficiency and higher compressor power. All variable condenser temperature testing data met AHRI stability and accuracy except the 32.6°C test point, where the energy balance metric was 4.04% and the AHRI limit was 3.69%.

The performance metrics are plotted as a percentage change compared to their baseline values. The overall COP and the thermal efficiency of the ORC increased as the condenser inlet temperature was decreased. Although more cooling was generated at lower condenser temperatures (322 kW at 16.6°C compared to 264 at 30°C), the greatly decreased compressor efficiency contributed to only a marginal increase in VCC COP (5.5% improvement at 16.6°C compared to baseline). When the condenser temperature was increased to 31.6°C and beyond, compressor stall was observed along with a steep drop in efficiency (67.7% at 31.6°C). The compressor efficiency during stall was higher than the compressor efficiency at the lowest condenser ambient temperature, which was an unexpected result. When the condenser inlet temperature was above 32.6°C, the compressor was surging and, thus, no data was collected

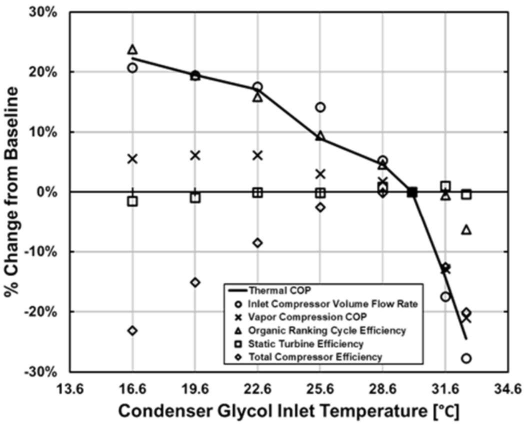


| *Condenser Inlet Temperature* | | | |
|---|---|---|---|
| | *16.6°C* | *30°C* | *32.6°C* |
| $COP_{TH}$ | 0.6816 | 0.5577 | 0.4211 |
| $COP_{VC}$ | 5.539 | 5.223 | 4.145 |
| $\eta_{ORC}$ | 9.541% | 7.706% | 7.218% |
| $\eta_{turb}$ | 75.54% | 76.70% | 76.37% |
| $\eta_{comp}$ | 65.12% | 84.75% | 67.72% |

**Fig. 5.** Performance of the ORVC test facility as a function of condenser glycol inlet temperature.

above this condenser temperature.

The turbine efficiency was nearly constant throughout the range of condenser temperatures, but the mass flow rate through the power cycle decreased slightly as the condenser temperature decreased. The mass flow rate through the power cycle was decreased to maintain 473 kW of heat input at 91°C because the enthalpy rise through the boiler was higher as condenser inlet temperature decreased. This phenomenon is shown in Fig. 6.: at the 16.6°C point, the enthalpy rise across the boiler is significantly higher (174.7 kJ $kg^{-1}$) compared to the 32.6°C test point (155.7 kJ $kg^{-1}$). To maintain the same 473 kW heat input (as designated by the AHRI standard), the mass flow rate through the power cycle must be decreased. Despite the slightly lower mass flow rate, the power output from the turbine was 15% higher at the lowest condenser inlet temperature compared to the baseline (57.71 kW compared to 50.07 kW). At 16.6°C condenser glycol inlet temperature, the condenser refrigerant saturation temperature was 26°C, compared to a refrigerant saturation temperature of 37°C when the condenser glycol inlet temperature was at

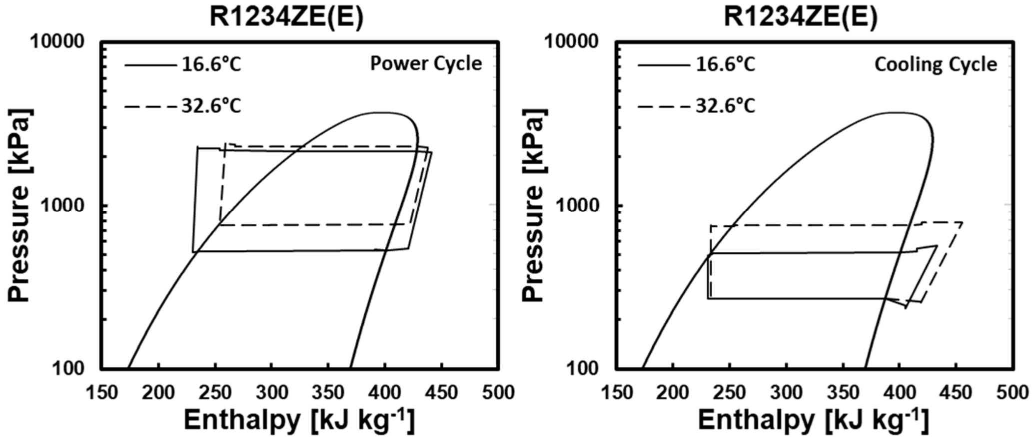


**Fig. 6.** P-h diagrams of the power and cooling cycles at the low and high condenser inlet temperatures.

the design point of 30°C. The higher power output was due to the higher pressure ratio across the turbine, which was 3.86 at 16.6°C compared to 3.03 at the baseline 30°C. The higher pressure ratio across the turbine can also be seen in Fig. 6.

When the turbine was generating more power at lower ambient temperatures, the compressor had more power to drive the cooling cycle which increased the refrigerant mass flow rate through the cooling cycle. Although higher cooling cycle mass flow rates increased the evaporator cooling duty, the compressor efficiency was significantly decreased because of the higher volumetric flow rate at the compressor inlet and an off-design pressure ratio. The volume flow rate changed as a function of condenser temperature, which pushes the compressor away from its highest efficiency point. For example, at the 16.6°C test point, the volume flow rate at the compressor inlet was 0.183 $m^3$ $s^{-1}$, compared to 0.152 $m^3$ $s^{-1}$ at the design point. In addition, the compressor pressure ratio was 2.38 when the condenser inlet temperature was 16.6°C while the standard design point for the compressor pressure ratio was 3.10. The lowered compressor pressure ratio is shown in Fig. 6. The increased volume flow rate and decreased pressure ratio pushed the compressor away from its ideal operating point, and, thus, the efficiency was much lower (65%) than the design point (84.8%).

### 3.3. Variable Chilled Water Delivery Temperature Results

The ORVC performance as a function of chilled water delivery temperatures from 2.1°C to 13.1°C is provided in Fig. 7. Although AHRI standards recommend testing chilled water delivery temperatures up to 21.1°C, the maximum test point was 13.1°C because the ORVC produced more chilling than was available from the heat source in the chilled water simulator loop. Steady state operation could not be maintained beyond 13.1°C chilled water delivery temperature. The baseline chilled water temperature was 7.0°C and yielded a thermal COP of 0.558. The chilled water temperature test points at 2.1°C, 3.1°C, and 5.1°C did not meet the condenser inlet temperature stability designated by AHRI. The condenser stability at 2.1°C, 3.1°C, and 5.1°C were 0.162°C, 0.14°C, and 0.158°C, respectively, which were slightly over the limit of 0.1°C from AHRI. In addition, at 11.1°C and 13.1°C chilled water delivery temperature, the chilled water temperature stability values were 0.12°C and 0.14°C, respectively, which exceeded the AHRI limit of 0.1°C.

The overall ORVC performance improved when the chilled water delivery temperature was raised. For example, when the chilled water temperature was 13.1°C, the thermal COP of the ORVC was 0.643 and the VCC COP was 6.169. Throughout the range of chilled water delivery temperatures, the thermal efficiency of the ORC and the turbine efficiency did not change more than 2%. The power cycle performance was largely unchanged because the boiler and condenser saturation pressures were extremely consistent throughout this range of tests. The economizer heat duty was nearly constant throughout the range of tests (from 47 kW at 2.1°C up to 42 kW at 13.1°C), despite an elevated compressor discharge temperature at lower chilled water delivery temperatures (86.0°C at 2.1°C delivery temperature compared to 67.1°C at 13.1°C delivery temperature). The economizer heat duty was nominally constant because the reduction in cooling cycle mass flow balanced out the increased compressor discharge temperature at low temperature chilled water delivery. The thermal COP of the ORVC generally followed the performance of the

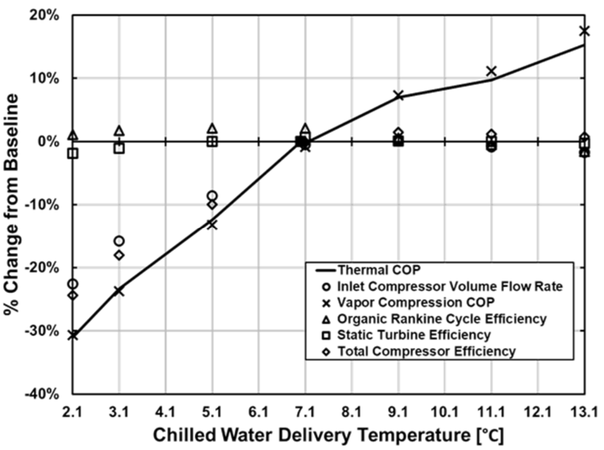


| ***Chiller Delivery Temperature*** | | | |
|---|---|---|---|
| | ***2.1°C*** | ***7°C*** | ***13.1°C*** |
| $COP_{TH}$ | 0.3845 | 0.5577 | 0.6430 |
| $COP_{VC}$ | 3.638 | 5.223 | 6.169 |
| $\eta_{ORC}$ | 7.791% | 7.706% | 7.586% |
| $\eta_{turb}$ | 75.25% | 76.70% | 76.49% |
| $\eta_{comp}$ | 64.08% | 84.75% | 85.38% |

**Fig. 7.** ORVC performance over a range of chilled water delivery temperature.

cooling cycle, as shown in Fig. 7.

The highest compressor efficiency, 85.97%, was achieved at a chilled water delivery temperature of 9.1°C. As the chiller saturation temperature decreased, the compressor pressure ratio increased and the inlet volumetric flow rate decreased, which caused a sharp decline in the efficiency of the compressor eventually resulting in compressor stall. The P-h diagram in Fig. 8 denotes the increased pressure ratio at lower chilled water delivery temperatures. At lower chilled water delivery temperatures, the cooling cycle mass flow rate decreased much more dramatically than

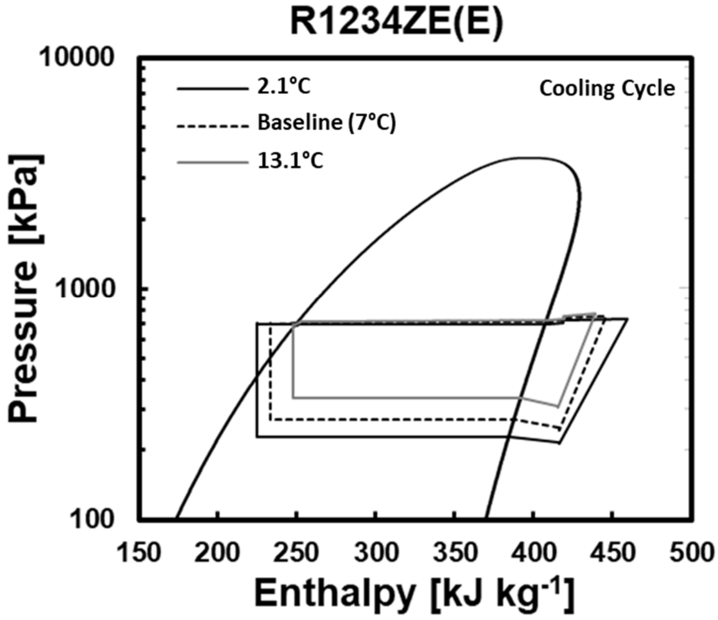


**Fig. 8.** P-h diagram of the vapor compression cycle at three chilled water delivery temperatures.

the compressor inlet density which negatively impacted the compressor performance. At 2.1°C, for example, the cooling cycle refrigerant mass flow rate was 33% lower than the baseline and the refrigerant density at the compressor inlet was 13.5% lower than the baseline. Thus, the inlet volumetric flow ($\dot{V} = \dot{m} / \rho$) to the compressor was reduced by 23% compared to the baseline case. The reduced volume flow and increased pressure ratio reduced the efficiency of the compressor to 64.1% as it approached stall. In contrast, as the chilled water delivery temperature was increased above the baseline case, the refrigerant density and mass flow changed at nearly the same rate, which maintained the volume flow rate. At 13.1°C, the refrigerant density at the compressor inlet was 25.9% higher than the baseline case and the mass flow was 23.7% higher than the baseline, which yielded only a 2% change in the inlet volumetric flow rate. Although the pressure ratio was decreased, the compressor maintained high efficiency during operation at elevated chilled water delivery temperatures. At 13.1°C, the efficiency of the compressor was 85.4%, which was very close to the baseline efficiency of 84.8%. Another interesting result of chilled water delivery temperature testing was that the SLHX provided less subcooling to the liquid side as the chilled water delivery temperature increased. At the baseline case with 7°C chilled water delivery temperature, the outlet temperature of the SLHX liquid side was 24.1°C, which yielded 13.2°C of subcooling. At the 13.1°C delivery temperature, the outlet temperature of the refrigerant from the liquid side of the SLHX was 34.6°C, which was only 3.2°C of subcooling. This was primarily a result of the condenser being undersized. The refrigerant mass flow rate through the cooling cycle at 7°C chilled water delivery temperature was 1.74 kg s$^{-1}$ which yielded a condenser outlet quality of 0.061. When the chilled water delivery temperature was increased to 13.1°C, the mass flow rate of the cooling cycle refrigerant increased to 2.15 kg s$^{-1}$ and the condenser outlet quality increased to 0.122. Thus, the SLHX could provide less subcooling as the chilled water delivery temperature increased because it had a higher fraction of the latent heat of the refrigerant to overcome. In addition, there was less thermal driving force for heat transfer as the temperatures of the streams on each side of the SLHX were much closer together when the chilled water delivery temperature was increased.

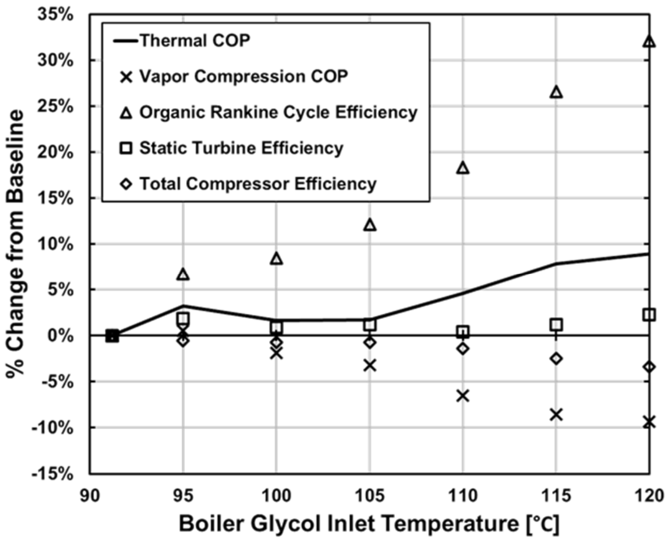


| *Boiler Inlet Temperature* | | |
|---|---|---|
| | ***91°C*** | ***120°C*** |
| $COP_{TH}$ | 0.5577 | 0.6075 |
| $COP_{VC}$ | 5.223 | 4.761 |
| $\eta_{ORC}$ | 7.706% | 10.18% |
| $\eta_{turb}$ | 76.70% | 78.44% |
| $\eta_{comp}$ | 84.75% | 81.90% |

**Fig. 9.** Performance trends for the ORVC over a range of heat source inlet temperatures.

### 3.4. Boiler Glycol Inlet Temperature Results

The performance trends for the ORVC as a function of boiler glycol inlet temperature are shown in Fig. 9. The boiler temperatures were varied from 91°C to 120°C, which was the maximum temperature rating for the loop. As the boiler temperature increased, the thermal COP increased, with a maximum COP of 0.608 at the boiler temperature of 120°C. All boiler temperature tests met the AHRI stability and accuracy criteria. As the boiler glycol temperature was increased while maintaining the same heat input, the refrigerant became more superheated at the turbine inlet as shown in Fig. 10. The ORC thermal efficiency increased along with the boiler inlet temperature, up to 10.2% at 120°C. The improved thermal efficiency in the ORC resulted from the increased enthalpy drop across the turbine which increased the power output (from 50.1 kW at the baseline to 62.9 kW at 120°C). The turbine efficiency was nearly constant throughout the range of boiler temperature tests.

The VCC COP decreased as the boiler inlet temperature was increased which was a result of economizing heat exchanger performance and the undersized cooling cycle condenser. At 120°C, the COP of the VCC was 4.76 compared to 5.223 at the baseline testing. Since the turbine outlet temperature was significantly higher during the high temperature boiler testing, the recuperator heat duty greatly increased and the liquid outlet temperature was significantly higher. Thus, the economizer heat duty had less thermal driving force and the heat duty decreased. For example, at 120°C the heat duty of the economizer was 20.2 kW compared to 46.4 kW at the baseline boiler inlet temperature of 91°C. Since less heat was rejected from the compressor discharge in the

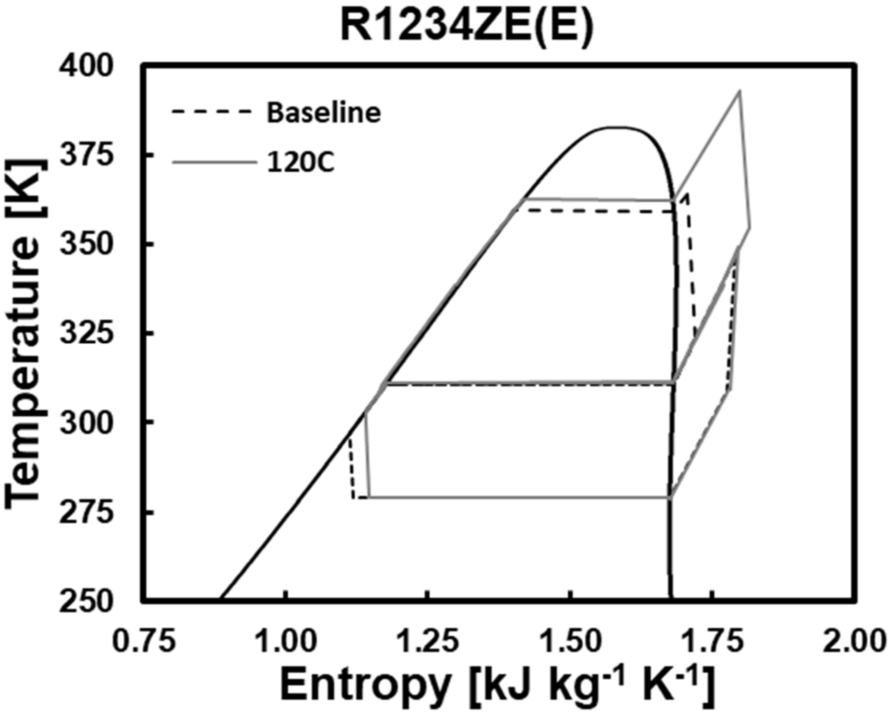


**Fig. 10.** T-s diagrams of power and cooling cycles at the baseline and 120°C boiler inlet temperature.

economizer, the cooling cycle condenser had to reject a greater amount of heat. During baseline testing, the refrigerant at the cooling cycle condenser outlet was two-phase with a vapor quality of 0.061, implying the cooling cycle condenser was already undersized. The reduction in heat duty of the economizer exasperated the challenges with the cooling cycle condenser and the outlet vapor quality of the condenser increased to 0.11 when the boiler inlet temperature was 120°C. This phenomenon carried through to the evaporator inlet, where the inlet vapor quality was higher (0.182) than the baseline (0.138), which can be seen in Fig. 10. The increased inlet vapor mass quality to the evaporator directly reduced the chilling capacity and COP of the VCC. Further increases to boiler inlet temperature could cause the power cycle fluid to reject heat to the cooling cycle in the economizer, which would hamper performance.

### 3.5. Integrated Part Load Value Testing

The ORVC was also tested in accordance with AHRI 551/591 to determine the IPLV. During part load testing, the temperatures of the external streams were altered to account for heat exchanger fouling, as designated in the standard. Thus, the 100% load test results are slightly different than the baseline testing. To achieve part load performance, the power cycle mass flow rate was decreased until the chilling load matched the desired part-load target. For example, at the 75% load condition, the power cycle mass flow rate was decreased from 3.15 kg $s^{-1}$ to 1.83 kg $s^{-1}$ and the boiler heat input was lowered to 275.5 kW (from 473 kW at the unfouled full load test). This resulted in a turbine power decrease from 50.1 kW to 27.6 kW. Thus, the compressor power decreased and the evaporator cooling duty decreased from 263.8 kW to 198.3 kW. In all part load testing, the external loop flow rates were maintained, the chilled water delivery temperature was maintained at 7°C, the boiler glycol inlet temperature was maintained at 91°C, and the condenser loop inlet temperature was adjusted according to Table 2. Since the flow rates of the external streams were maintained, as the evaporator load was decreased, the chilled water inlet temperature decreased and the boiler glycol outlet temperature increased. In all cases, the AHRI data criteria were met and the evaporator load was held to within 2% of the target values. The IPLV was calculated to be 0.682, which was a good representation of annualized

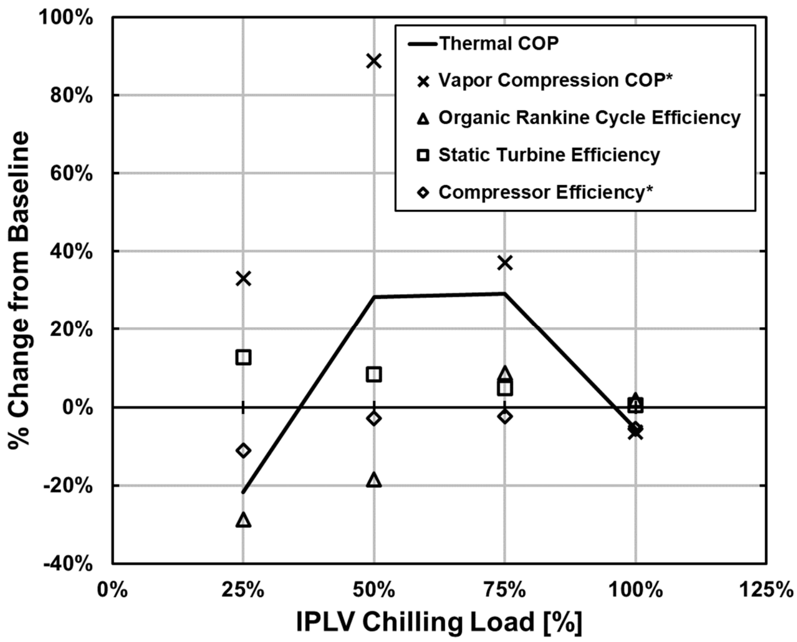


**Fig. 11.** Performance trends for part-load testing of the ORVC test facility.

performance for the ORVC.

A summary of the part-load test results is provided in Fig. 11 and Table 4. The highest ORVC thermal COP of 0.720 was found at the 75% load condition, which was calculated as designated by the standard with the external loop heat input and chilling output. At this load, the economizer heat exchanger had a significantly lower heat duty (4.3 kW at 75% load compared to 46.4 kW at 100% load) but the recuperator heat duty was higher (62.5 kW at 75% load compared to 35.5 kW at 100% load). The recuperator heat duty was higher because there was more superheat at the turbine inlet (26.2°C of superheat at 75% compared to 5°C of superheat at 100% load) which was due to a reduction in boiler saturation pressure (1415 kPa at 75% load compared to 2264 kPa at 100% load). The high side power cycle pressure and power cycle flow rate could not be independently controlled: as the flow rate was reduced to match the 75% load condition, the high side pressure was also reduced. Additional superheat at turbine inlet during the 75% load test point also increased the amount of sensible energy (65°C compared to 51°C at 100% load) at the turbine outlet, which increased the amount of heat transfer in the recuperator (62.5 kW at 75% load compared to 35.5 kW at 100% load). The turbine had higher efficiency than the baseline

(80.5% isentropic at 75% load versus 76.7% isentropic at 100% load). The ORC efficiency and the VCC COP were both higher at 75% load than 100% load, due in part to the more favorable condenser temperatures on both cycles (24.5°C at 75% load compared to 30°C at 100% load). The second highest overall ORVC COP was found at 50% load (0.716). Although the VCC COP was higher at 50% than 75%, the overall ORVC COP was lower at the 50% point because the ORC efficiency decreased sharply at 50% load. The ORC efficiency was much lower as a result of reversed heat flow in the economizer, which decreased power output from the turbine.

Although the turbine and compressor had high efficiency at the 50% load condition, the economizer was inhibiting power cycle performance by transferring heat from the power cycle to

**Table 4.**
Performance metrics from IPLV testing of the ORVC system.

| | ***Baseline*** | ***100%*** | ***75%*** | ***50%*** | ***25%*** |
|---|---|---|---|---|---|
| $COP_{TH}$ | 0.5577 | 0.526 | 0.720 | 0.716 | 0.436 |
| $COP_{VC}$ | 5.223 | 4.92 | 7.20 | 9.92 | 6.98 |
| $\eta_{ORC}$ | 7.71% | 7.85% | 8.38% | 6.28% | 5.49% |
| $\eta_{turb}$ | 76.7% | 77.1% | 80.5% | 83.1% | 86.5% |
| $\eta_{comp}$ | 84.8% | 80.1% | 82.8% | 82.4% | 75.4% |
| $\eta_{ORVC,2nd}$ | 27.2% | 26.5% | 24.6% | 15.5% | 9.5% |

the cooling cycle prior to the boiler inlet. At the 25% load, the economizer once again transferred heat from the VCC to the ORC because the power cycle economizer inlet was at a lower temperature than the two-phase cooling cycle economizer stream. An energy balance on the economizer could not be used to calculate the part-load mass flow rates on the cooling cycle because the economizer heat duty was very low at 75% load, negative at 50% load, and the fluid was two-phase at 25% load. Since the cooling cycle mass flow rate was unknown, the VCC COP was estimated using the turbine power output assuming 100% shaft efficiency. In addition, the static properties were used for compressor efficiency calculation since total properties could not be determined without the cooling cycle mass flow rate.

The primary cause for the ORC thermal efficiency decrease at 50% and 25% loads was the pressure ratio of the power cycle. As mentioned earlier, the power cycle pump speed and saturation pressure could not be independently controlled. To decrease the evaporator chilling load, the power cycle pump speed was decreased to reduce the power input to the cooling cycle. A byproduct of decreasing the pump speed was also a decrease in the high-side ORC saturation pressure, which significantly reduced the turbine power output. Thus, the ORC thermal efficiency decreased from 8.38% to 5.49% as the load was decreased from 75% to 25%, as shown in Fig. 11.

The compressor also began to stall at the 50% and 25% loads which was a result of the small amount of power output from the turbine. At 50% load, the compressor was absorbing 13.5 kW of power from the turbine which was simply not enough to overcome the pressure ratio of 1.849. This phenomenon was worse at 25% load. Despite compressor stall, the cooling cycle still generated 65.4 kW of chilled water at 25% load and 133.4 kW of chilled water at 50% load, which yielded an ORVC COP of 0.436 and 0.716, respectively.

The cooling cycle condenser performed better at part load. As mentioned earlier in this work and in the prior study, the cooling cycle condenser was too undersized to fully subcool the refrigerant during full load operation, resulting in an outlet vapor quality of 0.061 at full load [5]. During 75% load, the outlet vapor quality decreased to 0.048 and it was fully subcooled during 50% and 25% load. Full subcooling of the refrigerant at the condenser outlet vastly improved the VCC cycle COP, as shown in Fig. 11.

The 2$^{nd}$ Law efficiency was the actual ORVC COP divided by the maximum theoretical ORVC COP based on the high temperature, medium temperature, and low temperature auxiliary glycol streams. To determine the maximum theoretical COP of the ORVC, the glycol inlet temperatures for the boiler and condenser heat exchanger were used, while the evaporator water outlet temperature was used. The 100% load point had the highest 2$^{nd}$ Law efficiency at 27%. As the condenser inlet temperature decreased, the maximum theoretical COP of the ORVC system increased. Although the actual COP improved as well, the max theoretical COP increased more dramatically which decreased the 2$^{nd}$ Law efficiency.

## 4. Conclusions and Future Work

An ORVC system was tested over a range of conditions to analyze the impact of external stream temperatures on the system performance. The thermal COP of the ORVC improved as the condenser inlet temperature decreased, from 0.558 at 30°C to 0.682 at 16.6°C condenser inlet temperature. Although more chilling was produced, the compressor efficiency decreased along with condenser temperature which was due to higher refrigerant mass flow rates and pressure drop through the cooling cycle. The compressor efficiency was worse at lower condenser temperatures than during stall, a phenomenon that could not be captured by parametric simulations and would be difficult to predict with advanced, multi-dimensional turbomachinery models. Increasing the chilled water delivery temperature improved the COP of the ORVC: the COP raised from 0.558 at the baseline 7.0°C delivery temperature up to 0.643 when the delivery temperature was 13.1°C. Changing the chilled water delivery temperature had almost no impact on the ORC – the thermal efficiency of the power cycle did not change across the range of 2.1°C to 13.1°C delivery temperatures. The compressor efficiency was relatively constant as the temperature was increased above 7°C, but sharply decreased when the chilled water delivery temperature was below 7°C, which was another somewhat unexpected phenomenon that could only be captured with experimental verification. As the boiler glycol temperature was increased, the thermal efficiency of the ORC increased (up to 10.2%) and COP of the ORVC increased (up to 0.608). Surprisingly, the COP of the VCC decreased as the boiler glycol temperature increased, which was a result of the impacted economizer efficacy and a reduction in compressor efficiency. The compressor efficiency was reduced because of the increased cooling cycle mass flow and increased pressure ratio. The ORVC could not be operated below 91°C at full-load due to turbine flow choking.

In addition, the integrated part load value (IPLV) of the ORVC was 0.682. The COP of the ORVC was highest at 50% and 75% load because the VCC had a higher COP than baseline and the turbine efficiency was higher than the baseline case. Compressor stall was observed during the 50% and 25% loading tests because the compressor was not receiving enough power from the turbine and the blade design was not optimized for these conditions. The power cycle mass flow rate and the high side saturation pressure both changed as a function of pump speed and thus could not be controlled independently.

Future work will remediate the auxiliary loop challenges to extend the range of ORVC performance characterization. Additional strategies must be incorporated to avoid compressor stall at low loads and high pressure ratios. The data collected in this study will help generate performance maps for the turbomachinery, calibrate technoeconomic models, develop control algorithms, and contribute to design optimization studies. In addition, continued experimental efforts will characterize the performance of the test facility under transient loads.

**Credit authorship contribution statement**

**Alex Grauberger:** Methodology, Investigation, Writing – original draft. **Derek Young:** Investigation, Writing – original draft, review and editing. **Todd Bandhauer:** Supervision.

**Declaration of interests**

The authors declare that they have no known competing financial interests or personal relationships that could have appeared to influence the work reported in this paper.

☒ The authors declare the following financial interests/personal relationships which may be considered as potential competing interests:

Todd Bandhauer reports a relationship with Harvest Cooling that includes: board membership, consulting or advisory, employment, and equity or stocks. Todd Bandhauer has patent #10,294,826 issued to Colorado State University Research Foundation. Todd Bandhauer has patent #20210156597 pending to Colorado State University Research Foundation.

**Acknowledgements**

The authors would like to thank the U.S. Department of Energy's Office of Energy Efficiency and Renewable Energy (EERE) for its financial support under contract DE-EE0008325. Additionally, the authors would like to acknowledge project partners Barber Nichols Inc. and

Modine Manufacturing, Christian Dahm, Ben Platt, Kaitlyn Baker, Katie Plese, and Brandi Grauberger for their support in system design, test facility development, and experimentation.

## 5. References

[1] U.S. Energy Information Administration. Monthly Energy Review, April 2021. 2021.
[2] Manufacturing Energy and Carbon Footprint. 2019.
[3] Emissions C. Manufacturing Energy and Carbon Footprint. US Department of Energy 2014.
[4] Rattner AS, Garimella S. Energy harvesting, reuse and upgrade to reduce primary energy usage in the USA. Energy 2011. https://doi.org/10.1016/j.energy.2011.07.047.
[5] Grauberger A, Young D, Bandhauer T. Experimental Validation of an Organic Rankine-Vapor Compression Cooling Cycle using Low GWP Refrigerant R1234ze(E). Applied Energy 2022.
[6] Performance Rating of Water-chilling and Heat Pump Water-heating Packages Using the Vapor Compression Cycle AHRI 551/591. 2020.
[7] Trane. CenTraVac Water-cooled Liquid Chillers. 2020.
[8] Kim KH, Perez-Blanco H. Performance analysis of a combined organic Rankine cycle and vapor compression cycle for power and refrigeration cogeneration. Applied Thermal Engineering 2015;91. https://doi.org/10.1016/j.applthermaleng.2015.04.062.
[9] Li H, Bu X, Wang L, Long Z, Lian Y. Hydrocarbon working fluids for a Rankine cycle powered vapor compression refrigeration system using low-grade thermal energy. Energy and Buildings 2013;65:167–72. https://doi.org/10.1016/j.enbuild.2013.06.012.
[10] Bu XB, Li HS, Wang LB. Performance analysis and working fluids selection of solar powered organic Rankine-vapor compression ice maker. Solar Energy 2013;95:271–8. https://doi.org/10.1016/j.solener.2013.06.024.
[11] Yue C, You F, Huang Y. Thermal and economic analysis of an energy system of an ORC coupled with vehicle air conditioning. International Journal of Refrigeration 2016;64:152–67. https://doi.org/10.1016/j.ijrefrig.2016.01.005.
[12] Molés F, Navarro-Esbrí J, Peris B, Mota-Babiloni A, Kontomaris K. Thermodynamic analysis of a combined organic Rankine cycle and vapor compression cycle system activated with low temperature heat sources using low GWP fluids. Applied Thermal Engineering 2015;87. https://doi.org/10.1016/j.applthermaleng.2015.04.083.
[13] Prigmore D, Barber R, Co BE, Ave W. Cooling with the sun's heat. Journal of Solar Energy 1975. https://doi.org/10.1016/0038-092X(75)90058-4.
[14] Biancardi FR, Sitler JW, Melikian G. Development and test of solar Rankine cycle heating and cooling systems. International Journal of Refrigeration 1982;5. https://doi.org/10.1016/0140-7007(82)90057-3.
[15] Wang H, Peterson R, Harada K, Miller E, Ingram-Goble R, Fisher L, et al. Performance of a combined organic Rankine cycle and vapor compression cycle for heat activated cooling. Energy 2011;36. https://doi.org/10.1016/j.energy.2010.10.020.
[16] Demierre J, Favrat D, Schiffmann J, Wegele J. Experimental investigation of a Thermally Driven Heat Pump based on a double Organic Rankine Cycle and an oil-free Compressor-Turbine Unit. International Journal of Refrigeration 2014;44. https://doi.org/10.1016/j.ijrefrig.2014.04.024.
[17] Garland SD, Noall J, Bandhauer TM. Experimentally validated modeling of a turbo-compression cooling system for power plant waste heat recovery. Energy 2018. https://doi.org/10.1016/j.energy.2018.05.048.
[18] Liang Y, Mckeown A, Yu Z, Alshammari SFK. Experimental study on a heat driven refrigeration system based on combined organic Rankine and vapour compression cycles. Energy Conversion and Management 2021;234:113953. https://doi.org/10.1016/J.ENCONMAN.2021.113953.

[19] Sero Pump Systems - SRZS Pump. Https://SeropumpsCom/Srzs/ n.d.
[20] Lemmon EW, Bell IH, Huber ML, McLinden MO. NIST Standard Reference Database 23: Reference Fluid Thermodynamic and Transport Properties-REFPROP 2018.
[21] Akasaka R. New fundamental equations of state with a common functional form for 2,3,3,3-tetrafluoropropene (R-1234yf) and trans-1,3,3,3-tetrafluoropropene (R-1234ze(E)). International Journal of Thermophysics 2011;32. https://doi.org/10.1007/s10765-011-0992-0.
[22] ASME PTC 19.1-2018. Test Uncertainty. 2018.
[23] Performance Rating for Absoprtion Water Chilling and Water Heating Packages AHRI 560-2000. 2000.